Available online at www.sciencedirect.com
SCIENCE DIRECT®
Journal of Computational Physics 210 (2005) 705–729
JOURNAL OF COMPUTATIONAL PHYSICS
www.elsevier.com/locate/jcp

Finite volume treatment of dispersion-relation-preserving and optimized prefactored compact schemes for wave propagation

Mihaela Popescu [a], Wei Shyy [a,b,*], Marc Garbey [c]

[a] Department of Mechanical and Aerospace Engineering, University of Florida, Gainesville, FL 32611, United States
[b] Department of Aerospace Engineering, University of Michigan, Ann Arbor, MI 48109, United States
[c] Department of Computer Science, University of Houston, Houston, TX 77204, United States

Received 3 August 2004; received in revised form 11 May 2005; accepted 11 May 2005
Available online 12 July 2005

Abstract

In developing suitable numerical techniques for computational aero-acoustics, the dispersion-relation-preserving (DRP) scheme by Tam and co-workers and the optimized prefactored compact (OPC) scheme by Ashcroft and Zhang have shown desirable properties of reducing both dissipative and dispersive errors. These schemes, originally based on the finite difference, attempt to optimize the coefficients for better resolution of short waves with respect to the computational grid while maintaining pre-determined formal orders of accuracy. In the present study, finite volume formulations of both schemes are presented to better handle the nonlinearity and complex geometry encountered in many engineering applications. Linear and nonlinear wave equations, with and without viscous dissipation, have been adopted as the test problems. Highlighting the principal characteristics of the schemes and utilizing linear and nonlinear wave equations with different wavelengths as the test cases, the performance of these approaches is documented. For the linear wave equation, there is no major difference between the DRP and OPC schemes. For the nonlinear wave equations, the finite volume version of both DRP and OPC schemes offers substantially better solutions in regions of high gradient or discontinuity.

1. Introduction

In computational aero-acoustics (CAA) accurate prediction of the generation of sound is demanding due the requirement of preserving the shape and frequency of wave propagation and generation. Furthermore, the numerical schemes need to handle multiple scales, including long and short waves, and nonlinear

* Corresponding author. Tel.:+1 352 392 0961; fax: +1 352 392 7303.
E-mail address: weishyy@umich.edu (W. Shyy).

0021-9991/$ - see front matter © 2005 Elsevier Inc. All rights reserved.
doi:10.1016/j.jcp.2005.05.011

Nomenclature

c	sound speed
CFL	Courant–Friedrichs–Lewy number $= c\frac{\Delta t}{\Delta x}$
D_i	derivative in point i (Eq. (35))
D_i^{F}, D_i^{B}	forward and backward derivative operators in the point i (Eqs. (24)–(26), (33), (34))
E	error (Eqs. (4), (27), (78)–(80))
fd	finite difference
fv	finite volume
$K^{(i)}$	function computed in the stage i, in the Runge–Kutta time integration (Eqs. (46), (47))
Pe	Peclet number $= \frac{U\Delta x}{\mu}$
s_i, e_{N-i}	coefficients used to compute the derivative operator on the boundary, for OPC scheme (Eq. (33), (34), (37), (38))
t	time
u_i^{Be}, u_i^{Fe}	forward and backward operators computed on east face in the cell i (Eqs. (29)–(32), (57)–(60), (66)–(69))
$u_i^{\mathrm{Bw}}, u_i^{\mathrm{Fw}}$	forward and backward operators computed on west face in the cell i (Eqs. (29)–(32), (57)–(60), (66)–(69))
u_i^{e}	the value of parameter u on face e, in cell i (Eqs. (35), (36), (55), (56), (89), (91))
u_i^{w}	the value of parameter u on face w, in cell i (Eqs. (35), (36), (55), (56), (89), (91))
$u^{(m)}$	the value of function u in the stage m in the Runge–Kutta time integration (Eqs. (46), (47))
u^n	the value of function u in the n iteration, it is related to time integration (Eqs. (41), (42), (46), (47))
x, y	coordinate in space
Δx, Δy, Δt	length of grid in space, in x and y directions, respectively, time step size
$\bar{\alpha}$,	wavenumber of a space marching scheme (Eqs. (3), (4), (27))
α	wavenumber (Eqs. (3), (70))
μ	viscosity (Eqs. (92)–(96))
ω^*	angular frequency (Eqs. (42), (43), (72), (73))
$()^{\mathrm{F}}$, $()^{\mathrm{B}}$	parameter designed for forward, respectively, backward operator (Eqs. (25), (26), (37), (38))

governing laws arising from sources such as turbulence, shocks, interaction between fluid flows and elastic structures, and complex geometries. It is well recognized [1–3] that in order to conduct satisfactory CAA, numerical schemes should induce minimal dispersion and dissipation errors. In general, higher-order schemes would be more suitable for CAA than the lower-order schemes since, overall, the former are less dissipative. That is why higher-order spatial discretization schemes have gained considerable interest in computational acoustics [4–6]. Table 1 summarizes several approaches proposed in the literature.

For longer wavelengths, the formal order of accuracy is sufficient to indicate the performance of a scheme. However, for shorter waves relative to the grid size, it is known that the leading truncation error terms are not good indicators [7,8]. To handle broad band waves, the idea of optimizing the scheme coefficients via minimizing the truncation error associated with a particular range of wave numbers has been used over the years by many researchers, e.g. [9–16]. A successful approach is the dispersion-relation-preserving (DRP) finite difference scheme proposed by Tam and co-workers [2,3]. The basic idea in the DRP scheme is to optimize coefficients to satisfactorily resolve short waves with respect to the computational grid, namely, waves with wavelengths of 6–8Δx (defined as 6–8 points per wave or PPW) or shorter. It maximizes the accuracy by matching the wave number and frequency characteristics between the

Table 1
The computational cost for DRP and OPC schemes

Scheme	The philosophy of the scheme	Applications
DRP [2,3]	In this scheme a central difference is employed to approximate first derivative. The coefficients are optimized to minimize a particular type of error	Wave propagation
LDDRK [9,10]	Traditionally, the coefficients of the Runge–Kutta scheme are optimized to minimize the dissipation and propagation waves. The optimization does not compromise the stability consideration	Wave propagation problem
LDFV [11,12]	Scheme minimizes the numerical dispersion errors that arise in modeling convection phenomena, while keeping dissipation errors small. This is accomplished by special high-order polynomials that interpolate the properties at the cell centers to the left and right sides of cell faces. A low pass filter has been implemented to remove high frequency oscillation near shock waves	Shock noise prediction
GODPR [13]	It is derived, based on optimization that gives finite difference equations locally the same dispersion relation as the original partial differential equations on the grid points in the nonuniform Cartesian or curvilinear mesh	Used for geometry, that rectangular grid is not appropriate: • Acoustic radiation from an oscillating circular cylinder in a wall • Scattering of acoustic pulse from a cylinder • Acoustic wave propagation
OWENO [14]	The idea is to optimize WENO in wave number schemes, following the practice of DRP scheme to achieve high resolution for short wave. But in the same time it retains the advantage of WENO scheme in that discontinuity are captured without extra numerical damping.	Simulation of the shock/broadband acoustic wave
CE/SE [26,27]	The method is developed by imposing that: (i) space and time to be unified and treated as a single entity; (ii) both local and global flux conservation in space and time to be enforced; (iii) multidimensional scheme to be constructed without using the dimensional-splitting approach	Flow involving shock; acoustic wave
FDo, RKo [38]	Optimized schemes are obtained by similar approach as DRP (space discretization), respectively LDDRK (time discretization). The difference consists that: (i) error is minimized taking into account logarithm of the wavenumber; (ii) the error is minimized on an interval that starts from $\ln(\pi/16)$. The stability and accuracy increase for these schemes	(a) convective wave equation (b) subsonic flows past rectangular open cavities; (c) circular jet

analytical and the numerical operators in the range of resolvable scales. Recently, Ashcroft and Zhang [15] have reported a strategy for developing optimized prefactored compact (OPC) schemes, requiring smaller stencil support than DRP. The prefactorization strategy splits the central implicit schemes into forward and backward biased operators. Using Fourier analysis, they have shown that it is possible to select the coefficients of the biased operators such that their dispersion characteristics match those of the original central compact scheme. Hixon and Turkel [17] proved that the ''prefactored scheme is equivalent to the initial compact scheme if: (i) the real components of forward and backward operators are equal to those at the corresponding wavenumber of the original compact scheme; (ii) the imaginary components of the forward and backward operators are equal in magnitude and opposite in sign.

Both DRP and OPC schemes are originally designed based on the finite difference approach. In order to satisfy the governing laws of the fluid physics, it can be advantageous to adopt the finite volume approach [18–20], which ensures that fluxes estimated from different sides of the same surface are identical, i.e., no

spurious source/sink is generated due to numerical treatment. Such a requirement is particularly important when nonlinearity is involved, as is typically the case in shock and turbulence aspects of the aero-acoustic computations. Furthermore, a finite volume formulation can offer an easier framework to handle the irregular geometry and moving boundaries. In this work, we extend the concept embodied in the original, finite difference-based DRP scheme (which we call DRP-fd) to a finite volume formulation (which we call DRP-fv). Similarly, for the OPC-scheme, we extend the basic concepts of the original, finite difference-based OPC (OPC-fd) scheme, to a finite volume formulation, called OPC-fv. Our overall goal is to develop the finite volume version of DRP and OPC schemes utilizing a cut-cell type of Cartesian-grid techniques and numerical treatments suitable for aero-acoustic problems. Papers relevant to these aspects can be found in Refs. [19–34].

In this paper, we present the finite volume formulation of both DRP and OPC schemes, and assess both fd and fv versions of the DRP and OPC schemes, using well defined test problems to facilitate systematic evaluations. Both linear and nonlinear wave equations with different wavelengths and viscous effects are utilized for direct comparisons. In the following, we first summarize the essence of the individual schemes, including derivations, then present assessment of the test cases.

2. Numerical schemes

In the following we use the following one-dimensional wave equation to facilitate the development and presentation of the concept and numerical procedures:

$$\frac{\partial u}{\partial t} + c\frac{\partial u}{\partial x} = 0. \tag{1}$$

The equation contains time and space derivative. In our work the space derivative term is treated with either DRP or OPC scheme, and the time derivative by a low-dissipation and low-dispersion Runge–Kutta (LDDRK) scheme [9], to be discussed later.

In Section 2.1, we first summarize the original finite difference procedure of DRP. In Section 2.2, we present the finite volume version of DRP. The boundary treatment of the DRP schemes is presented in Section 2.3.

The OPC scheme is the second method considered for the space derivative. The finite difference procedure of the OPC scheme is offered in Section 2.4. The extension of this approach to a finite volume framework is presented in 2.5. The specific boundary treatment of OPC schemes is given in 2.6.

In Section 2.7, the LDDRK scheme [9] is presented. As mentioned earlier, this scheme is used to approximate time derivative in all treatment trough.

2.1. Discretization in space – The finite difference-based DRP scheme (DRP-fd)

Consider the simple one-dimensional wave equation. In [2,3], the discretization in space is given by:

$$\frac{\partial u}{\partial x}(x) \cong \frac{1}{\Delta x}\sum_{j=-N}^{N} a_j u(x + j\Delta x), \tag{2}$$

where Δx is the space grid, and coefficients a_j are constant. This approach is based on two goals: (i) the behavior of the numerical solution in the resolvable wavenumber range closely matches that of the exact solution, and (ii) the formal order of accuracy of scheme spanning $2N + 1$ nodes is $2(N - 1)$.

To obtain the value of the wave number of the scheme the author used the Fourier transform and shift theorems

$$\bar{\alpha} = -\frac{\mathrm{i}}{\Delta x}\sum_{j=-N}^{N} a_j \mathrm{e}^{\mathrm{i}j\alpha\Delta x}. \tag{3}$$

The goal is to ensure that $\bar{\alpha}$ (wavenumber of the scheme) is as close to α as possible. To accomplish this goal the error is minimized over a certain wavenumber range, $\alpha\Delta x \in [-\eta;\eta]$ – the numerical dispersion is reduced by specifying the range of optimization [2,3]

$$E = \int_{-\eta}^{\eta} |\alpha\Delta x - \bar{\alpha}\Delta x|^2 \,\mathrm{d}(\alpha\Delta x). \tag{4}$$

It is noted that $\bar{\alpha}$ is real, and hence the coefficients a_j must be anti-symmetric, i.e.,

$$a_0 = 0 \quad \text{and} \quad a_{-j} = -a_j. \tag{5}$$

On substituting Eq. (3) into Eq. (4), and taking Eq. (5) into account, E can be written as,

$$E = \int_{-\eta}^{\eta} \left[\lambda - 2\sum_{j=1}^{N} a_j \sin(\lambda \cdot j)\right]^2 \mathrm{d}\lambda, \tag{6}$$

where $\lambda = \alpha\Delta x$.

The coefficients are determined by imposing a certain order of accuracy to the scheme, and minimizing the error E.

2.2. The finite volume-based DRP scheme (DRP-fv)

To incorporate the DRP-fd concept into a finite volume framework, let us consider a one-dimensional linear wave equation:

$$\frac{\partial\phi}{\partial t} + c\frac{\partial\phi}{\partial x} = 0. \tag{7}$$

To derive the discretized equation, we employ the grid point cluster shown in Fig. 1. We focus on the grid point i, which has the grid points $i-1$, and $i+1$ as its neighbors. The dashed lines define the control volume and letters e and w denote east and west faces, respectively, of the control volume. For the one-dimensional problem under consideration, we assume a unit thickness in the y and z directions; thus, we obtain

$$\int_{\mathrm{e}}^{\mathrm{w}} \frac{\partial\phi}{\partial t}\,\mathrm{d}x + c((A\phi)_{\mathrm{e}} - (A\phi)_{\mathrm{w}}) = 0, \tag{8}$$

where $(A\phi)_{\mathrm{e}}$ and $(A\phi)_{\mathrm{w}}$ are the flux across the east and west faces, respectively.

Hence, the discretized wave equation (7) can be written as

$$\frac{\partial\bar{\phi}}{\partial t}\Delta x + c((A\phi)_{\mathrm{e}} - (A\phi)_{\mathrm{w}}) = 0, \tag{9}$$

where $\bar{\phi}$ is the averaged value of ϕ over a control volume.

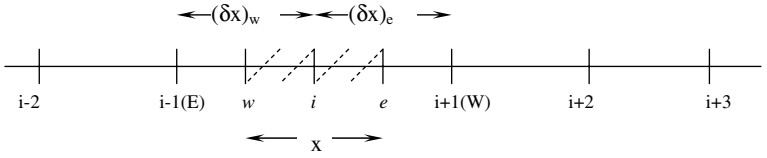

Fig. 1. Grid points cluster for one-dimensional problem.

Taking into account Eq. (9), we describe the general form of the approximation of $\frac{\partial\phi}{\partial x}$ in 1D using the control volume concept:

$$\frac{\partial\phi}{\partial x} \to \frac{1}{\Delta x}((\phi A)_{\mathrm{e}} - (\phi A)_{\mathrm{w}}). \tag{10}$$

The general form of the DRP scheme is:

$$\left(\frac{\partial\phi}{\partial x}\right)_l \cong \frac{1}{\Delta x}\sum_{k=-3}^{k=3} a_k \phi_{l+k}, \tag{11}$$

where Δx is the space grid, and coefficients a_j are constant.

The DRP scheme has a general form similar to the central difference approximation. Hence, one can adopt a central difference scheme to express ϕ_{e} in the neighborhood:

$$(\phi)_{\mathrm{e}} = \beta_1\phi_{i-2} + \beta_2\phi_{i-1} + \beta_3\phi_i + \beta_4\phi_{i+1} + \beta_5\phi_{i+2} + \beta_6\phi_{i+3}, \tag{12}$$

$$(\phi)_{\mathrm{w}} = \beta_1\phi_{i-3} + \beta_2\phi_{i-2} + \beta_3\phi_{i-1} + \beta_4\phi_i + \beta_5\phi_{i+1} + \beta_6\phi_{i+2}. \tag{13}$$

Taking into consideration Eqs. (10)–(13) we obtain the values of the β_i, $i = 1,\ldots,6$ by imposing that the value of ϕ at the same locations has the same values as that of the DRP-fd.

$$\sum_{k=-3}^{k=3} a_k \phi_{l+k} = \phi_{\mathrm{e}} - \phi_{\mathrm{w}}. \tag{14}$$

Hence, the values of coefficients β's are

$$\begin{cases} \beta_1 = \beta_6 = a_3, \\ \beta_2 = \beta_5 = a_2 + a_3, \\ \beta_3 = \beta_4 = a_1 + a_2 + a_3. \end{cases} \tag{15}$$

To illustrate the above-described concept, we consider the following equation:

$$\frac{\partial u}{\partial t} + c_1\frac{\partial u}{\partial x} + c_2\frac{\partial u}{\partial y} = 0. \tag{16}$$

If we integrate Eq. (16) on the surface we have (see Fig. 2):

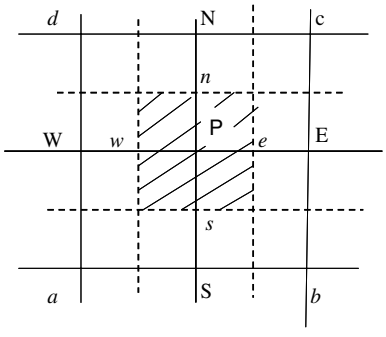

Fig. 2. Grid notation for two-dimensional problem, where (i) P denotes the center of a cell, (ii) E, W, N, and S denote, respectively, the nodes corresponding to the east, west, north and south neighbors, (iii) e, w, n and s denote, respectively, the center of the east, west, north and south faces of the cell, and (iv) *a*, *b*, *c*, and *d* denote, respectively, the corners of the cell.

$$\int_V \frac{\partial u}{\partial t}\,\mathrm{d}v + \oint c_1 u\,\mathrm{d}y - c_2 u\,\mathrm{d}x = \frac{\partial u}{\partial t} s_{abcd} + c_1(u_\mathrm{s}\Delta y_\mathrm{s} + u_\mathrm{e}\Delta y_\mathrm{e} + u_\mathrm{n}\Delta y_\mathrm{n} + u_\mathrm{w}\Delta y_\mathrm{w}) + c_2(-u_\mathrm{s}\Delta x_\mathrm{s} - u_\mathrm{e}\Delta x_\mathrm{e} - u_\mathrm{n}\Delta x_\mathrm{n} - u_\mathrm{w}\Delta x_\mathrm{w}). \tag{17}$$

The resulting DRP-fv scheme is:

$$\frac{\partial \bar{u}}{\partial t} = \frac{1}{S_{abcd}} F_{i,j}, \tag{18}$$

where

$$F_{i,j} = -[c_1(u^s_{i,j}\Delta y_\mathrm{s} + u^\mathrm{e}_{i,j}\Delta y_\mathrm{e} + u^n_{i,j}\Delta y_\mathrm{n} + u^\mathrm{w}_{i,j}\Delta y_\mathrm{w}) + c_2(u^s_{i,j}\Delta x_\mathrm{s} + u^\mathrm{e}_{i,j}\Delta x_\mathrm{e} + u^n_{i,j}\Delta x_\mathrm{n} + u^\mathrm{w}_{i,j}\Delta x_\mathrm{w})], \tag{19}$$

$$u^\mathrm{e}_{i,j} = \beta_1 u_{i-2,j} + \beta_2 u_{i-1,j} + \beta_3 u_{i,j} + \beta_4 u_{i+1,j} + \beta_5 u_{i+2,j} + \beta_6 u_{i+3,j}, \tag{20}$$

$$u^\mathrm{w}_{i,j} = \beta_1 u_{i-3} + \beta_2 u_{i-2,j} + \beta_3 u_{i-1,j} + \beta_4 u_{i,j} + \beta_5 u_{i+1,j} + \beta_6 u_{i+2,j}, \tag{21}$$

$$u^n_{i,j} = \beta_1 u_{i,j-2} + \beta_2 u_{i,j-1} + \beta_3 u_{i,j} + \beta_4 u_{i,j+1} + \beta_5 u_{i,j+2} + \beta_6 u_{i,j+3}, \tag{22}$$

$$u^s_{i,j} = \beta_1 u_{i,j-3} + \beta_2 u_{i,j-2} + \beta_3 u_{i,j-1} + \beta_4 u_{i,j} + \beta_5 u_{i,j+1} + \beta_6 u_{i,j+2}. \tag{23}$$

2.3. The boundary treatment of the DRP scheme

The current version of the DRP scheme requires seven grid points in space. Consequently, it is necessary to impose some supplementary condition for boundary treatments. In this regard, Tam et al. [2] devise ghost points. The minimum number of ghost points is equal to the number of boundary conditions. For example, for an inviscid flow the condition of no flux through the wall requires a minimum of one ghost value per boundary point on the wall. It is desirable to use a minimum number of ghost points to maintain simplicity in coding and structuring data.

In this paper, we use only backward difference for grid points near the computational boundary and a ghost point is used only for wall boundary condition.

2.4. The finite difference-based optimized prefactored compact (OPC-fd) scheme

To derive the factorized compact scheme, Ashcroft and Zhang [15] define forward and backward operators D_i^F and D_i^B, such that

$$\left(\frac{\partial u}{\partial x}\right)_i = \frac{1}{2}(D_i^\mathrm{B} + D_i^\mathrm{F}). \tag{24}$$

The generic stencil for the forward and backward derivative operators is then defined as:

$$\eta^\mathrm{F}\cdot D^\mathrm{F}_{i+1} + \beta^\mathrm{F}\cdot D^\mathrm{F}_i = \frac{1}{\Delta x}[a^\mathrm{F}\cdot u_{i+2} + b^\mathrm{F}u_{i+1} + c^\mathrm{F}\cdot u_i + d^\mathrm{F}\cdot u_{i-1} + e^\mathrm{F}u_{i-2}], \tag{25}$$

$$\beta^\mathrm{B}\cdot D^\mathrm{B}_i + \gamma^\mathrm{B}\cdot D^\mathrm{B}_{i-1} = \frac{1}{\Delta x}[a^\mathrm{B}\cdot u_{i+2} + b^\mathrm{B}u_{i+1} + c^\mathrm{B}\cdot u_i + d^\mathrm{B}\cdot u_{i-1} + e^\mathrm{B}u_{i-2}]. \tag{26}$$

The coefficients of the scheme are chosen such that: (i) the wavenumber of the scheme is close to the important wavenumber of the exact solution; (ii) the imaginary components of the forward and backward stencils are equal in magnitude and opposite in sign, and the real components are equal and identical to original compact scheme; (iii) the scheme preserves a certain order of accuracy. The authors [15] define the integrated error (weighted deviation) as:

$$E = \int_0^{r\pi} (\alpha\Delta x - \bar{\alpha}\Delta x) W(\alpha\Delta x)\, \mathrm{d}\alpha\Delta x, \tag{27}$$

where $W(\alpha\Delta x)$ is a weighting function, and r is a factor to determine the optimization range ($0 < r < 1$). The integrated error, defined in Eq. (27), is different from the one of Tam and Web [2] in that it contains the weighting function. The coefficients are obtained by imposing that, within a given asymptotic order, the error is minimal. In space discretization, one sacrifices formal order of accuracy in favor of wide-band performance, especially for the short wave components.

2.5. The finite volume-based OPC scheme (OPC-fv)

Taking into account Eq. (8) that describes the approximation of the first derivative in the finite volume formulation, equations that describe the OPC scheme, Eqs. (25 and 26), and the idea that the general form of approximation of the function for points at the center of the cell face, namely, e and w assumes similar forms:

$$\begin{cases} u_{\mathrm{e}} = 0.5(u^{\mathrm{Fe}} + u^{\mathrm{Be}}), \\ u_{\mathrm{w}} = 0.5(u^{\mathrm{Fw}} + u^{\mathrm{Bw}}), \end{cases} \tag{28}$$

where u^{Fe}, u^{Be}, u^{Fw} and u^{Bw} are determined from:

$$\eta u_{i+1}^{\mathrm{Fe}} + \beta u_i^{\mathrm{Fe}} = b u_{i+1} - d u_i, \tag{29}$$

$$\eta u_{i+1}^{\mathrm{Fw}} + \beta u_i^{\mathrm{Fw}} = b u_i - d u_{i-1}, \tag{30}$$

$$\beta u_i^{\mathrm{Be}} + \eta u_{i-1}^{\mathrm{Be}} = b u_i - d u_{i+1}, \tag{31}$$

$$\beta u_i^{\mathrm{Bw}} + \eta u_{i-1}^{\mathrm{Bw}} = b u_{i-1} - d u_i, \tag{32}$$

where the coefficients are the same as those in the OPC-fd scheme: $\eta = \eta^{\mathrm{F}} = \gamma^{\mathrm{B}}$, $\beta = \beta^{\mathrm{F}} = \beta^{\mathrm{B}}$, $b = b^{\mathrm{F}} = -d^{\mathrm{B}}$, $d = = d^{F} = -b^{\mathrm{B}}$. These relationships among forward and backward operators are obtained by Ashcroft and Zhang [15].

2.6. The boundary treatment of the OPC scheme

Boundary formulation of the OPC scheme employs a biased explicit stencil. Ashcroft and Zhang [15] design OPC-fd scheme with the following boundary stencil:

$$D_1^{\mathrm{B}} = \frac{1}{\Delta x} \sum_{j=1}^{4} s_j u_j, \quad D_N^{\mathrm{B}} = \frac{1}{\Delta x} \sum_{j=N-3}^{N} e_j u_j \tag{33}$$

and

$$D_1^{\mathrm{F}} = \frac{1}{\Delta x} \sum_{j=1}^{4} -e_{N+1-j} u_j, \quad D_N^{\mathrm{F}} = \frac{1}{\Delta x} \sum_{j=N-3}^{N} -s_{N+1-j} u_j, \tag{34}$$

where the coefficients s_j and e_j are determined by matching the Taylor series of the forward and backward compact interior stencils to third-order accuracy.

The boundary treatment in case of OPC-fv approach is similar to that of OPC-fd, but the boundary stencil is computed on the face:

$$D_i = (uA)_i^{\mathrm{e}} - (uA)_i^{\mathrm{w}}, \tag{35}$$

$$\begin{cases} u_1^{\mathrm{w}} = \sum_{i=1}^{3} a_i u_i, \\ u_1^{\mathrm{e}} = \sum_{i=1}^{3} a_i u_{i+1}, \end{cases} \quad \begin{cases} u_N^{\mathrm{w}} = \sum_{i=1}^{3} r_i u_{N-i}, \\ u_N^{\mathrm{e}} = \sum_{i=1}^{3} r_i u_{N-i+1}, \end{cases} \tag{36}$$

where the values of the coefficients are:

$$\begin{cases} a_1^{\mathrm{B}} = -s_1, \\ a_2^{\mathrm{B}} = -s_1 - s_2, \\ a_3^{\mathrm{B}} = -s_1 - s_2 - s_3, \end{cases} \quad \begin{cases} a_1^{\mathrm{F}} = e_N, \\ a_2^{\mathrm{F}} = e_N + e_{N-1}, \\ a_3^{\mathrm{F}} = e_N + e_{N-1} - e_{N-2}, \end{cases} \tag{37}$$

$$\begin{cases} r_1^{\mathrm{B}} = e_N, \\ r_2^{\mathrm{B}} = e_N + e_{N-1}, \\ r_3^{\mathrm{B}} = e_N + e_{N-1} - e_{N-2}, \end{cases} \quad \begin{cases} r_1^{\mathrm{F}} = -s_1, \\ r_2^{\mathrm{F}} = -s_1 - s_2, \\ r_3^{\mathrm{F}} = -s_1 - s_2 - s_3. \end{cases} \tag{38}$$

2.7. Time discretization – The LDDRK method

Hu et al. [9] consider time integration using the Runge–Kutta algorithm of the differential equation

$$\frac{\partial u}{\partial t} = F(u), \tag{39}$$

where the operator F is a function of u. An explicit p-stage algorithm advances the solution of Eq. (39) from the nth to the $(n+1)$th iteration as

$$\begin{aligned} &u^{(0)} = u^n, \\ &K^{(1)} = \Delta t F(u^{(0)}), \\ &\cdots \\ &K^{(i)} = \Delta t F(u^{(i-1)}), \\ &u^{(i)} = u^n + b_i K^{(i)}, \quad i = 1, \ldots, p, \\ &\cdots \\ &u^{n+1} = u^{(p)}, \end{aligned} \tag{40}$$

where $b_p = 1$, $u^{(p)}$, where p indicates the stage in algorithm advances, and u^{n+1}, where n indicates the number of iterations for time dependent computation.

The value of the u^{n+1} can be written on short like

$$u^{n+1} = u^n + \sum_{j=1}^{p} \underbrace{\prod_{l=p-j+1}^{p} b_l}_{=\gamma_j} \Delta t^j \frac{\partial^j u^n}{\partial t^j}. \tag{41}$$

The resulting algorithm is obtained by optimizing the dispersion and dissipation properties. Assuming $F(u)$ is linear and applying temporal Fourier transform to (41), the amplification factor is given by

$$r = \frac{\tilde{u}^{n+1}}{\tilde{u}^n} = \left(1 + \sum_{j=1}^{p} \gamma_j (-\mathrm{i}\omega^* \Delta t)^j\right). \tag{42}$$

The exact amplification factor is

$$r_{\mathrm{e}} = \mathrm{e}^{-\mathrm{i}\omega^* \Delta t} = \mathrm{e}^{-\mathrm{i}\sigma}. \tag{43}$$

The numerical amplification factor r in (42) is viewed as an approximation of the exact factor. The order of the optimized Runge–Kutta scheme is indicated by the leading coefficient in (42) that matches the Taylor series expansion of $e^{-i\sigma}$. For instance, the third-order algorithm is obtained by setting $\gamma_j = 1/j!$ for $j = 1$, 2 and 3.

To compare the numerical and exact solutions we take into consideration the ratio:

$$\frac{r}{r_e} = |r|e^{-i\delta}, \tag{44}$$

where $|r|$ represents the dissipation rate (obviously, the correct value should be 1), and δ represents the phase error (or dispersive error) where the correct value should be 0.

Hu et al. [9] obtained coefficients of the LDDRK scheme by imposing that: (i) the scheme has certain order of accuracy, (ii) the error of the amplification factor of the scheme is minimized, which means that both dispersion and dissipation errors are minimized. In other words the following integral is minimized:

$$\int_0^\Gamma \left| 1 + \sum_{j=1}^{p} c_j(-i\sigma)^j - e^{-i\sigma} \right|^2 d\sigma = \min \tag{45}$$

and (iii) the amplification factor of the scheme is less than one within the given stability limit.

In this work we use a two-step alternating scheme: in odd steps we use four stages and in the even steps we use six stages. The scheme is a fourth-order accurate scheme in time for a linear problem and second-order accurate for a nonlinear problem. The advantage of the alternating schemes is that, when two steps are combined, the dispersion and the dissipation errors can be reduced and higher-order of accuracy can be maintained. The specific procedure is given below.

1. *Four-stage*

$$\begin{aligned}
K^{(1)} &= \Delta t F(u^n),\\
K^{(2)} &= \Delta t F\left(u^n + \frac{1}{4}K^{(1)}\right),\\
K^{(3)} &= \Delta t F\left(u^n + \frac{1}{3}K^{(2)}\right),\\
K^{(4)} &= \Delta t F\left(u^n + \frac{1}{2}K^{(3)}\right),\\
u^{n+1} &= u^n + K^{(4)}.
\end{aligned} \tag{46}$$

2. *Six-stage*

$$\begin{aligned}
K^{(1)} &= \Delta t F(u^n),\\
K^{(2)} &= \Delta t F(u^n + 0.17667K^{(1)}),\\
K^{(3)} &= \Delta t F(u^n + 0.38904K^{(2)}),\\
K^{(4)} &= \Delta t F\left(u^n + \frac{1}{4}K^{(3)}\right),\\
K^{(5)} &= \Delta t F\left(u^n + \frac{1}{3}K^{(4)}\right),\\
K^{(6)} &= \Delta t F\left(u^n + \frac{1}{2}K^{(5)}\right),\\
u^{n+1} &= u^n + K^{(6)}.
\end{aligned} \tag{47}$$

In the following we will give an implementation example of LDDRK scheme when we use OPC and DRP schemes for space discretization. Based on Eq. (1), the value of F in point l is defined as follows:

- *DRP-fd*:

$$F_l = -\frac{c}{\Delta x}\sum_{i=-3}^{3} a_i u_{l+i}. \tag{48}$$

- *DRP-fv*:

$$F_l = -c(u_l^{\mathrm{e}} - u_l^{\mathrm{w}})/\Delta x, \tag{49}$$

where

$$u_l^{\mathrm{e}} = \beta_1 u_{l-2} + \beta_2 u_{l-1} + \beta_3 u_l + \beta_4 u_{l+1} + \beta_5 u_{l+2} + \beta_6 u_{l+3}, \tag{50}$$
$$u_l^{\mathrm{w}} = \beta_1 u_{l-3} + \beta_2 u_{l-2} + \beta_3 u_{l-1} + \beta_4 u_l + \beta_5 u_{l+1} + \beta_6 u_{l+2}. \tag{51}$$

In the linear case, the fv and fd schemes are equivalent.

- *OPC-fd*:

$$F_l = -\frac{c}{2}(D_l^{\mathrm{B}} + D_l^{\mathrm{F}}), \tag{52}$$

where D_l^{B} and D_l^{F} are obtained from the following system of equations:

$$\eta D_{i+1}^{\mathrm{F}} + \beta D_i^{\mathrm{F}} = \frac{1}{\Delta x}[b(u_{i+1} - u_i) + d(u_{i-1} - u_i)], \quad i = 1, \ldots, N, \tag{53}$$
$$\beta D_i^{\mathrm{B}} + \eta D_{i-1}^{\mathrm{B}} = \frac{1}{\Delta x}[d(u_i - u_{i+1}) + b(u_i - u_{i-1})], \quad i = 1, \ldots, N, \tag{54}$$

where N represent the number of grid points in space.

- *OPC-fv*:

$$F_l = -c(u_l^{\mathrm{e}} - u_l^{\mathrm{w}})/\Delta x, \tag{55}$$

where

$$u_l^{\mathrm{e}} = 0.5(u_l^{\mathrm{Be}} + u_l^{\mathrm{Fe}}), \quad \text{and} \quad u_l^{\mathrm{w}} = 0.5(u_l^{\mathrm{Bw}} + u_l^{\mathrm{Fw}}). \tag{56}$$

The value of u_l^{Be}, u_l^{Fe}, u_l^{Bw}, u_l^{Fw} are obtained by solving the following system of equations:

$$\eta u_{i+1}^{\mathrm{Fe}} + \beta u_i^{\mathrm{Fe}} = b u_{i+1} - d u_i, \quad i = 1, \ldots, N, \tag{57}$$
$$\eta u_{i+1}^{\mathrm{Fw}} + \beta u_i^{\mathrm{Fw}} = b u_i - d u_{i-1}, \quad i = 1, \ldots, N, \tag{58}$$
$$\beta u_i^{\mathrm{Be}} + \eta u_{i-1}^{\mathrm{Be}} = b u_i - d u_{i+1}, \quad i = 1, \ldots, N, \tag{59}$$
$$\beta u_i^{\mathrm{Bw}} + \eta u_{i-1}^{\mathrm{Bw}} = b u_{i-1} - d u_i, \quad i = 1, \ldots, N. \tag{60}$$

3. Analytical assessment of DRP and OPC schemes

3.1. Operation counts

We will compare the cost between the alternative approaches only for the approximation of the first derivative, because we employ the same time stepping scheme for both scheme.

The efficient form of general formula for the discretization in space of the DRP-fd scheme is:

$$F_i = \frac{1}{\Delta x}[a_3(x_{i+3} - x_{i-3}) + a_2(x_{i+2} - x_{i-2}) + a_1(x_{i+1} - x_{i-1})]. \tag{61}$$

This scheme requires a total of three multiplications and five additions to evaluate the first derivatives in a certain point. In case of DRP-fv the most efficient form of the computations scheme is:

$$u_e = \frac{1}{\Delta x}[\beta_1(u_{i+3} + u_{i-2}) + \beta_2(u_{i+2} + u_{i-1}) + \beta_3(u_i + u_{i+1})], \tag{62}$$

$$u_w = \frac{1}{\Delta x}[\beta_1(u_{i-3} + u_{i+2}) + \beta_2(u_{i-2} + u_{i+1}) + \beta_3(u_i + u_{i-1})]. \tag{63}$$

DRP-fv requires a greater number of operations than DRP-fd: 6 multiplications and 11 additions to compute the first derivatives at a given point.

To see the computational cost of the OPC-fd scheme we adopt the most efficient form that is:

$$\frac{1}{2}D_i^F = \frac{1}{2\beta\Delta x}[b(u_{i+1} - u_i) + d(u_{i-1} - u_i)] - \frac{\eta}{2\beta}D_{i+1}^F, \tag{64}$$

$$\frac{1}{2}D_i^B = \frac{1}{2\beta\Delta x}[b(u_i - u_{i-1}) + d(u_i - u_{i+1})] - \frac{\eta}{2\beta}D_{i-1}^B, \tag{65}$$

where the relation between the coefficients of the forward and backward stencils has been substituted to highlight the equivalent terms in the two stencils. The operation count is then four multiplications and five additions per point [15].

OPC-fv can be written in the form:

$$\frac{1}{2}D_i^F = \frac{1}{2\Delta x}(u_i^{Fe} - u_i^{Fw}), \tag{66}$$

$$\frac{1}{2}D_i^B = \frac{1}{2\Delta x}(u_i^{Be} - u_i^{Bw}), \tag{67}$$

where

$$\begin{cases} u_i^{Fe} = \frac{1}{\beta_F}[bu_{i+1} - du_i - \eta u_{i+1}^{Fe}], \\ u_i^{Fw} = \frac{1}{\beta}[bu_i - du_{i-1} - \eta u_{i+1}^{Fw}], \end{cases} \tag{68}$$

$$\begin{cases} u_i^{Be} = \frac{1}{\beta}[bu_i - du_{i+1} - \eta u_{i-1}^{Be}], \\ u_i^{Bw} = \frac{1}{\beta}[bu_{i-1} - du_i - \eta u_{i-1}^{Be}]. \end{cases} \tag{69}$$

In this case the operation count is 11 additions and 6 multiplications per point.

So we can see also in Table 2 the finite volume approach is computationally more expensive.

Table 2
The computational cost for DRP and OPC schemes

Scheme	Number of operation
DRP-fd	8
DRP-fv	17
OPC-fd	9
OPC-fv	17

3.2. Dispersive characteristics

The characteristics of the OPC and DRP schemes, in the finite difference form over the interval 0 to π, are shown in Fig. 3. One can see that the difference between the effective wave number of the scheme and the real wave is maintained to be within 2% if $\alpha\Delta x < 1.30$ for the DRP scheme, and $\alpha\Delta x < 1.84$ for the OPC scheme. The dispersive characteristics of these schemes can be more clearly seen in Fig. 4, which shows the phase speed error, $\mathrm{abs}(\frac{\mathrm{d}\bar{\alpha}\Delta x}{\mathrm{d}\alpha\Delta x} - 1)$, as a function of wave number on a log-arithmetic scale. We see that the DRP scheme has a somewhat larger error than the OPC scheme until around 3π/4. The error is maintained to be within 2% for $\alpha\Delta x$ less than 0.85 for the DRP scheme, and less than 1.53 for the OPC scheme. Overall, the OPC scheme yields slightly less dispersion error than the DRP scheme.

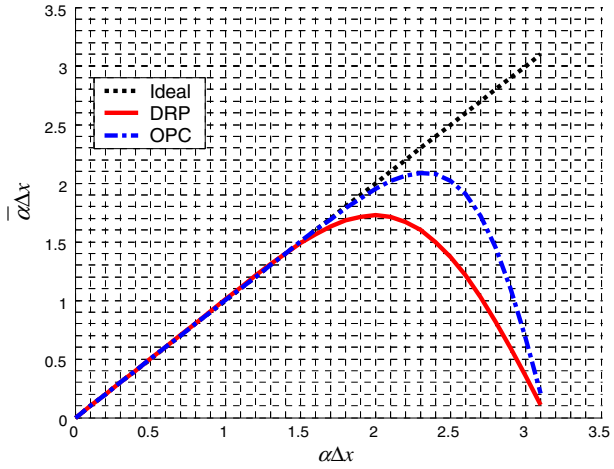

Fig. 3. Dispersive characteristics of the schemes.

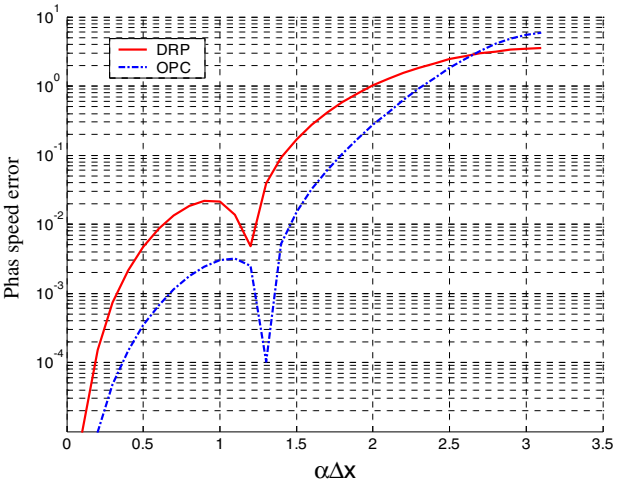

Fig. 4. Phase speed error on a logarithmic scale.

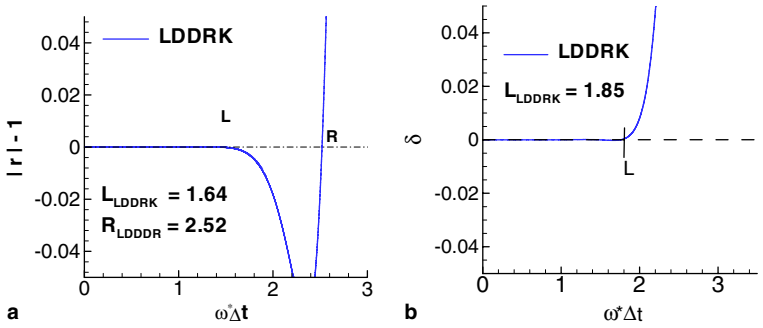

Fig. 5. Four–six-stage optimized Runge–Kutta of order four scheme: (a) dissipation error; (b) phase error.

The dispersive characteristics of LDDRK are obtained by studying the value of $|r|$ and δ, i.e., dissipation rate and dispersion error (see Eq. (44)), respectively. In Fig. 5 we can see conditions of stability: $|r| < 1$ for $\omega^*\Delta t \leqslant 2.52$. To obtain an accurate solution the dispersive characteristics ($|r|$ and δ) should be close to the exact solution ($|r|$ close to one and δ close to zero). Hu et al. [9] considered time accurate criterion $||r| - 1| \leqslant 0.001$ (i.e., $\omega^*\Delta t \leqslant 1.64$), and $\delta \leqslant 0.001$ (i.e., $\omega^*\Delta t \leqslant 1.85$). These two conditions are satisfied if $\omega^*\Delta t \leqslant 1.64$.

3.3. Stability of the schemes

The Fourier–Laplace transformation of the wave equation (Eq. (1)) is

$$-\mathrm{i}\omega^*\tilde{u} = -c\mathrm{i}\alpha\tilde{u} + \frac{1}{2\pi}\tilde{u}_{\text{initial}}, \tag{70}$$

where α, ω^* characterize the PDE. For the long wave we can approximate wavenumber of the scheme with wavenumber of the PDE

$$\bar{\alpha} \simeq \alpha, \tag{71}$$

which leads to

$$\omega^*\tilde{u} = c\bar{\alpha}\tilde{u} + k\tilde{u}_{\text{initial}}. \tag{72}$$

Hence

$$\omega^* = \bar{\alpha}c + kk. \tag{73}$$

The condition of the numerical stability is that amplification factor for time discretization is less than 1, and hence $\omega^*\Delta t \leqslant 2.52$ (see Fig. 5(a)). It is also noted from Fig. 3 that

$$\begin{aligned} &\bar{\alpha}\Delta x \leqslant 1.8 \quad \text{for DRP scheme,} \\ &\bar{\alpha}\Delta x \leqslant 2.1 \quad \text{for OPC scheme} \end{aligned} \tag{74}$$

hold true. By introducing Eq. (74) into (73) and upon multiplying by Δt it is found that

$$\begin{aligned} &\omega^*\Delta t \leqslant 1.8\frac{c}{\Delta x}[kk \cdot M + 1] \cdot \Delta t \quad \text{for DRP scheme,} \\ &\omega^*\Delta t \leqslant 2.1\frac{c}{\Delta x}[kk \cdot M + 1] \cdot \Delta t \quad \text{for OPC scheme,} \end{aligned} \tag{75}$$

where M is mach number. From Fig. 5(a) it is clear that the condition of stability is satisfied if $|\omega^*\Delta t|$ is less than 2.52. Therefore, to ensure numerical stability it is sufficient, by Eq. (75), to restrict Δt to be less than $\Delta t_{\max}$, where $\Delta\ t_{\max}$ is given by

$$\begin{aligned}\Delta t_{\max} &= \frac{2.52}{1.8[kk\cdot M+1]}\frac{\Delta x}{c} \quad \text{for DRP scheme,}\\ \Delta t_{\max} &= \frac{2.52}{2.1[kk\cdot M+1]}\frac{\Delta x}{c} \quad \text{for OPC scheme.}\end{aligned} \tag{76}$$

Therefore, for $\Delta\ t < \Delta t_{\max}$ the schemes are numerically stable. Consequently, the schemes yield the following criteria for numerical stability:

$$\begin{aligned}&\mathrm{CFL} < 1.4 \quad \text{for DRP scheme,}\\ &\mathrm{CFL} < 1.2 \quad \text{for OPC scheme.}\end{aligned} \tag{77}$$

Although it is clear that CFL $\leqslant 1.4$ is the stability condition for DRP scheme, this limit does not assure accuracy of the solution. In the previous analysis we have established that the solution is time accurate for 4–6 LDRRK if $\|r| - 1| \leqslant 0.001$ and $|\delta| \leqslant 0.001$. But this limit is not fixed, but depends on the scheme that is used for space discretization. For example, in the case of the DRP scheme, the solution is considered time accurate as long as $\|r| - 1| \leqslant 0.02$ and $|\delta| \leqslant 0.02$, or $\omega^* t \leqslant 2.0$. Hence, in this case the condition of being both accurate and stable is CFL $\leqslant 1.1$.

The OPC scheme is less sensitive to the dispersive characteristics of the LDDRK scheme; hence CFL < 1.2 is a condition of the stability and accuracy for the OPC scheme. This limit is in concordance with the stability analysis of Ashcroft and Zhang [15].

4. Computational assessment of the DRP and OPC schemes

To investigate the behavior of the schemes, we will use four test problems. First, we consider a one-dimensional wave equation with constant speed. The purpose of this test is to check the accuracy, stability, dissipation and dispersion of the scheme. The second test problem is a one-dimensional nonlinear wave equation with no viscous dissipation. The purpose of this test case is to (i) check the influence of singularities on the performance of the scheme, and (ii) analyze dispersion properties when waves are coupled. In the third test problem, we consider the one-dimensional viscous Burgers equation, which contains unsteady, nonlinear convection and viscous terms. In this case we pay attention to the influence of the viscosity on the solution accuracy. The last test problem is a 2D acoustic scattering problem from the second CAA Workshop [35]. This problem tests the curved wall boundary and the capacity of the scheme to reproduce different wavelengths.

To evaluate the solution accuracy, we define the error vector as:

$$\vec{E} = [E_1, \ldots, E_N]^{\mathrm{T}}, \tag{78}$$

where

$$E_i = U(x_i) - u_i, \quad 1 \leqslant i \leqslant N, \tag{79}$$

$U(x_i)$ is the exact solution at the point x_i, and u_i is the numerical solution at the point x_i. We choose to use the discrete L_1 norm:

$$\|E\| == \frac{\sum_{i=1}^{N}|E_i|}{N} \tag{80}$$

to measure the order of accuracy in our numerical computations.

4.1. Test problem 1: one-dimensional linear wave equation

To assess the behavior of the DRP and OPC schemes the following simple test problem is studied first.

$$\frac{\partial u}{\partial t} + c\frac{\partial u}{\partial x} = 0, \tag{81}$$

$$u = \exp\left[-\ln 2\left(\frac{x - x_0}{r}\right)^2\right] \quad \text{at } t = 0 \tag{82}$$

which is a Gaussian profile. This is one of the test problems offered in the second CAA Workshop [35].

The exact solution is:

$$U = \exp\left[-\ln 2\left(\frac{x - x_0 - ct}{r}\right)^2\right]. \tag{83}$$

In this study we evaluate the performance of the schemes in short, intermediate, and long waves relative to the grid spacing, which is assured by the value $r\Delta x$.

For time discretization, we previously presented the detailed formulas for the 4-6 LDDRK, see Eqs. (46 and 47).

Tam et al. [2,3] show that $\bar{\alpha}\Delta x$ is related to $\alpha\ \Delta x$, and in function of $\alpha\Delta x$ they divided the wave spectrum into two categories: (i) the long waves (waves for which $\bar{\alpha}\Delta x$, in this case $\alpha\Delta x$ is less than $\alpha\Delta x_c$), (ii) the short waves (waves for which $\bar{\alpha}$ is not close to α). This difference between long and short waves is totally dependent upon the grid space. Hence, by inspecting the number of grid points on the wavelength, we can decide that we have a certain category of wave.

In the following, we will present the results based on three categories:

- long wave ($r/\Delta x = 20$),
- intermediate wave ($r/\Delta x = 6$),
- short wave ($r/\Delta x = 3$).

The categories are defined according to the ratio $r/\Delta x$, where r is a parameter that characterizes the wavelength of this problem. This test problem is linear; hence we do not expect differences between finite difference and finite volume approach.

In regard to the time step selection, the CFL number (v) limit is similar for all schemes. We can see from Fig. 6 that the critical CFL number of both schemes is close to 1.1. From the study of the error in time for linear equations with constant convection speed it is clear that the DRP-fv and OPC-fv schemes have essentially the same behavior as the corresponding finite difference approach; hence, we only present comparison for DRP-fv and OPC-fv schemes.

The error decreases when the grid size in space decreases until a critical value is reached. For all schemes the errors have slopes consistent with the formal order of accuracy in space. This conclusion is confirmed in Fig. 7, where the CFL number is maintained at 0.5. For the long time scale solution, the accumulation of error for both DRP and OPC schemes is very close (as seen in Fig. 7(b)). Here, we consider: (i) different grid space, so both schemes have almost the same initial error and (ii) the same CFL number (0.5). This behavior is expected because both schemes present the same discretization in time. The DRP scheme presents a marginally faster accumulation of error in time.

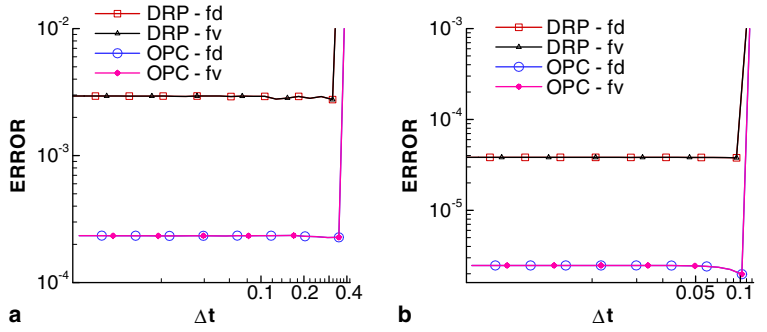

Fig. 6. Errors with respect to the time step size under a fixed space Δx, at $t = 50$ – linear wave equation. (a) $r/\Delta x = 3$ (short wave); (b) $r/\Delta x = 10$ (long wave).

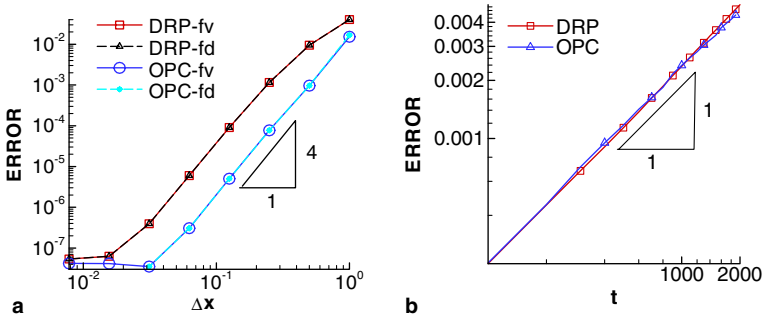

Fig. 7. Errors under a fixed CFL = 0.5, at $t = 50$ – linear wave equation: (a) error with respect to the space size; (b) accumulation of the error in time.

4.2. Test problem 2: one-dimensional nonlinear wave equation

The finite volume and finite difference schemes are equivalent for a linear equation. The difference between them appears for the nonlinear convective equation. To observe the merits and similarities of DRP and OPC schemes, we restrict ourselves to the 1D case. In this test, a nonlinear wave equation with a different speed is solved:

$$\frac{\partial u}{\partial t} + u\frac{\partial u}{\partial x} = 0. \tag{84}$$

This equation is solved in the conservative form:

$$\frac{\partial u}{\partial t} + 0.5\frac{\partial (u^2)}{\partial x} = 0. \tag{85}$$

To better understand the effect of high gradients and discontinuities, we chose the following initial conditions:

$$u(x,0) = \begin{cases} 0, & x \leqslant 0, \\ 1, & x > 0. \end{cases} \tag{86}$$

The solution for this problem can be written as:

$$u(x,t) = \begin{cases} 0, & x \leqslant 0, \\ \frac{x}{t}, & 0 < x < t, \\ 1, & x \geqslant t. \end{cases} \tag{87}$$

In this case, for both DRP and OPC schemes, the finite difference version behaves differently from the finite volume version. In Eqs. (46) and (47) the function F takes the form:

- *DRP-fd*

$$F_i = -0.5 \sum_{k=-3}^{3} a_k (u_{i+k})^2, \tag{88}$$

- *DRP-fv*

$$F_i = -0.5((u_i^{\mathrm{e}})^2 - (u_i^{\mathrm{w}})^2), \tag{89}$$

  where u_{e} and u_{w} are as defined before
- *OPC-fd*

$$F_i = -0.25(D_i^{\mathrm{B}} + D_i^{\mathrm{F}}), \tag{90}$$

  where D_i^{B} and D_i^{F} is backward and forward derivative of u^2 in place of u
- *OPC-fv*

$$F_i = -0.25((u_i^{\mathrm{e}})^2 - (u_i^{\mathrm{w}})^2), \tag{91}$$

  where u_{e} and u_{w} are defined by (57)–(60)

The similarities and differences for all three categories (short waves [$\Delta x/U = 1.0$], intermediate waves [$\Delta x/U = 0.25$], and long waves [$\Delta x/U = 0.06$]) are first presented. It should be noted again that the short, intermediate and long waves are defined based on the numerical resolution. Here, U is defined as the jump ($u_{\max} - u_{\min}$); in our case $U = 1$, hence in the following we discuss only the effect of the grid space step (Δx).

The evolution of the error as a function of grid spacing (Δx) is similar for both DRP and OPC schemes; the difference between the finite volume and finite difference versions are far greater, as shown in Fig. 8. In

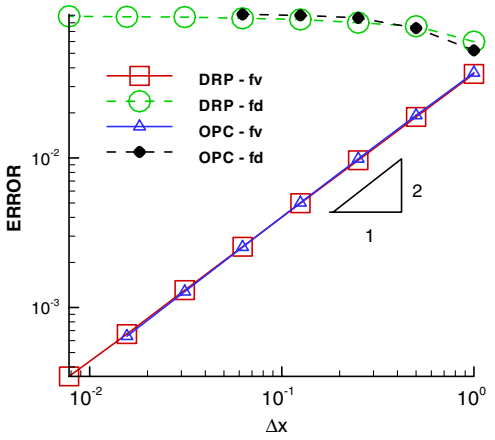

Fig. 8. Errors with respect to the space step size under a fixed CFL = 0.5, at $t = 5$ – nonlinear wave equation.

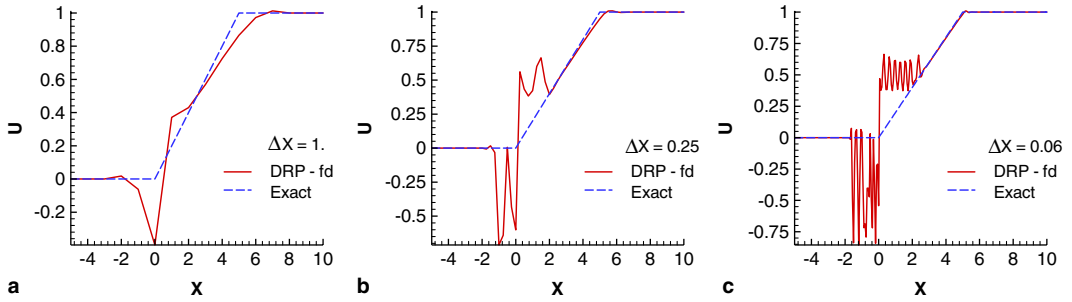

Fig. 9. DRP-fd solution – nonlinear wave equation; $t = 5$; CFL = 0.5. (a) $-\Delta x = 1$, (b) $-\Delta x = 0.25$, (c) $\Delta x = 0.06$.

the case of finite volume, error decreases with decreasing grid space. For finite difference, a totally different behavior is seen. The error not only does not decrease when grid spacing decreases, but in fact increases, as seen in Figs. 8, 9 and 11.

For short waves, all solutions show substantial errors, but the finite difference schemes perform noticeably worse. In the case of intermediate or long waves, the finite volume schemes exhibit satisfactory or better performance than the finite difference schemes (see Figs. 10 and 12).

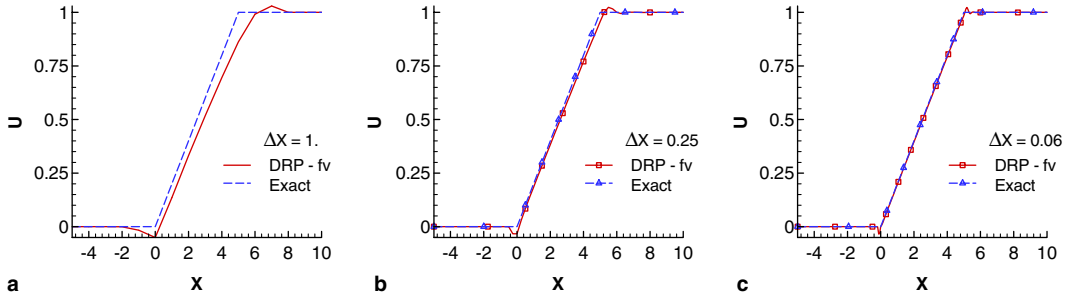

Fig. 10. DRP-fv solution – nonlinear wave equation; $t = 3$; CFL = 0.5. (a) $x = 1$, (b) $-\Delta x = 0.25$, (c) $\Delta x = 0.06$.

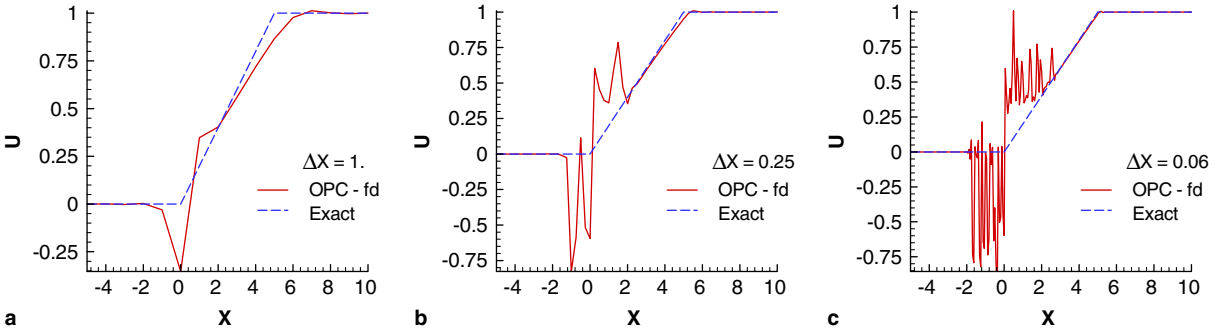

Fig. 11. OPC-fd solution – nonlinear wave equation; $t = 5$; CFL = 0.5. (a) $\Delta x = 1$, (b) $\Delta x = 0.25$, (c) $\Delta x = 0.06$.

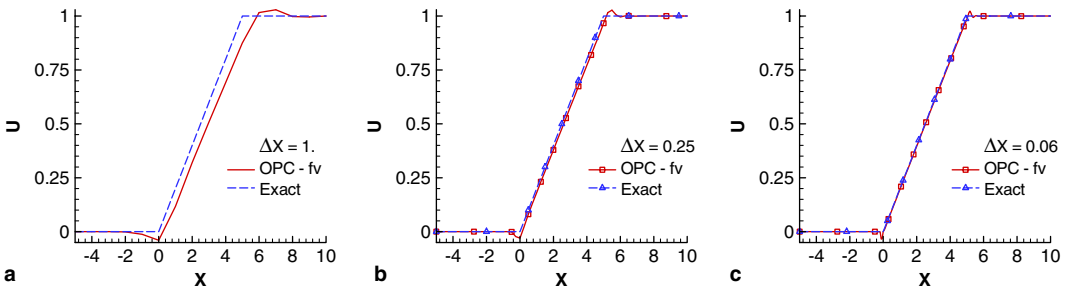

Fig. 12. OPC-fv solution – nonlinear wave equation; $t = 5$; CFL = 0.5. (a) $\Delta x = 1$, (b) $\Delta x = 0.25$, (c) $\Delta x = 0.06$.

4.3. Test problem 3: one-dimensional nonlinear Burgers equation

In this test the solution for the one-dimensional nonlinear Burgers equation is evaluated.

$$\frac{\partial u}{\partial t} + u\frac{\partial u}{\partial x} = \mu\frac{\partial^2 u}{\partial x^2}. \tag{92}$$

The numerical solution will approach Eq. (92) in conservative form:

$$\frac{\partial u}{\partial t} + 0.5\frac{\partial u^2}{\partial x} = \mu\frac{\partial^2 u}{\partial x^2}. \tag{93}$$

The initial condition is:

$$u(x,0) = 1 - \tanh\left(\frac{x - x_0}{2\mu}\right). \tag{94}$$

In this case the exact solution is:

$$u(x,t) = 1 - \tanh\left(\frac{x - x_0 - t}{2\mu}\right). \tag{95}$$

The scheme described earlier for inviscid Burgers' equation can also be applied to the current equation. This is accomplished by simply adding a second-order central difference expression for the viscous term u_{xx}. In other words F_i is replaced by H_i

$$H_i = F_i + \mu(u_{i-1} - 2u_i + u_{i-1})/\Delta x. \tag{96}$$

Because of the viscosity that characterizes the scheme in this case, it is expected that the solution of both approaches would be stable and similar. Hence this term will have a large influence over the value of the error.

In our discussion, we will distinguish the following three categories of results:

- short wave ($\Delta x/\mu = 10$),
- intermediate wave ($\Delta x/\mu = 3$),
- long wave ($\Delta x/\mu = 1$).

In this case the numerical performance is affected by two parameters: the CFL number and the Peclet number (Pe = $U\Delta x/\mu$).

First we compare the solution of all four schemes as function of the Peclet number (Pe) under constant CFL number (0.2). The value of CFL number is fixed at 0.2, because the critical value for all schemes is

much lower in the present case than for the linear case. The behavior of the error is similar among DRP-fv, DRP-fd, OPC-fd and OPC-fv: the error increases with increasing Peclet number, until a certain value beyond which the schemes can no longer perform satisfactorily.

For the four schemes (DRP-fv, DRP-fd, and OPC-fv, OPC-fd), the solution and error are very similar for all categories of wave, as shown in Figs. 13–15. For long waves the solution is reproduced with high accuracy with all four schemes, but the finite volume approach presents a slightly higher accuracy than the finite difference schemes. The error for the intermediate wave is nearly the same with all four approaches.

4.4. Test problem 4: two-dimensional acoustic scattering problem

To check the accuracy of the finite volume schemes in multi-dimensional situations, we consider a test problem from the Second CAA Workshop [35]: the two-dimensional acoustic scattering problem. The physical problem is to find the sound field generated by a propeller scattered off by the fuselage of an

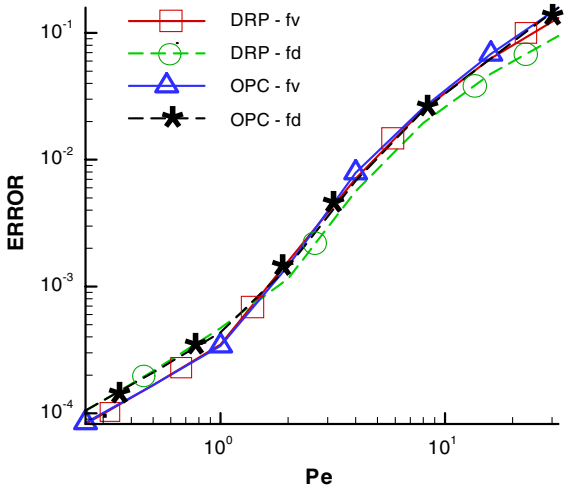

Fig. 13. Error in function of Pe – nonlinear Burgers equation; $\Delta x = 0.25$; CFL = 0.2; $t = 20$.

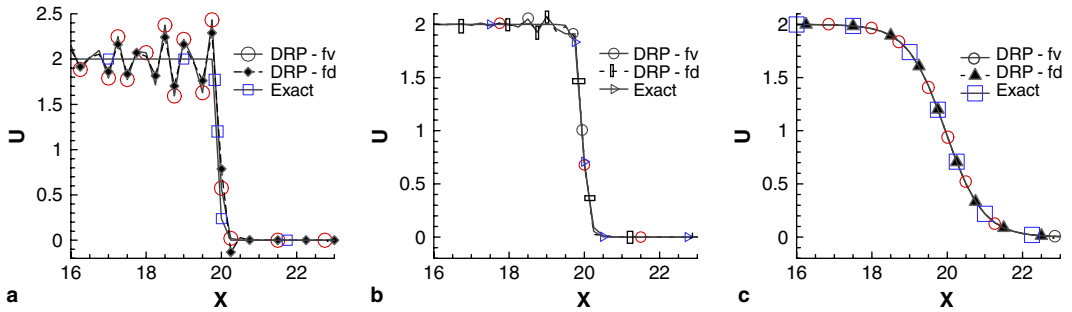

Fig. 14. Numerical solution obtained by DRP schemes – nonlinear Burgers equation; $\Delta x = 0.25$; CFL = 0.2; $t = 20$. (a) $Pe = 10$, (b) $Pe = 3$, (c) $Pe = 1$.

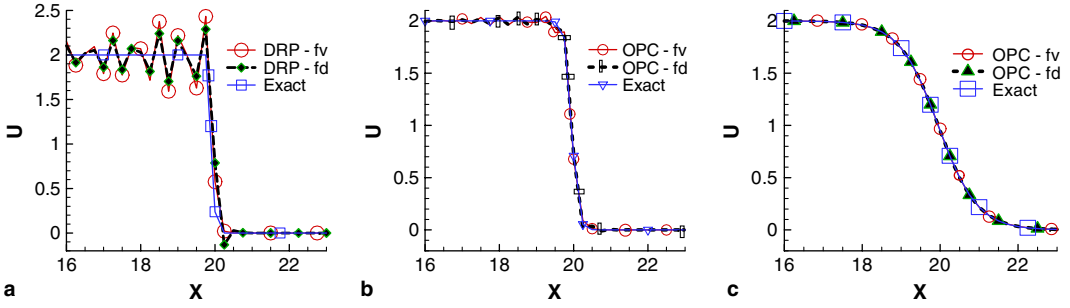

Fig. 15. Numerical solution obtained by OPC schemes – nonlinear Burgers equation; $\Delta x = 0.25$; CFL = 0.2; $t = 20$. (a) $Pe = 10$, (b) $Pe = 3$, (c) $Pe = 1$.

aircraft. The pressure loading on the fuselage is an input to the interior noise problem. The fuselage is idealized by a circular cylinder and the noise source (propeller) as a line source so that the computational problem is two-dimensional. The cylinder has a radius of $R = 0.5$ and is located at the center of the domain.

The linearized Euler equations in polar coordinates are:

$$\frac{\partial}{\partial t}\begin{bmatrix} u_r \\ u_\theta \\ p \end{bmatrix} + \frac{\partial}{\partial r}\begin{bmatrix} p \\ 0 \\ u_r \end{bmatrix} + \frac{1}{r}\frac{\partial}{\partial \theta}\begin{bmatrix} 0 \\ p \\ u_\theta \end{bmatrix} + \frac{1}{r}\begin{bmatrix} 0 \\ 0 \\ u_r \end{bmatrix} = \begin{bmatrix} 0 \\ 0 \\ 0 \end{bmatrix}. \tag{97}$$

At time $t = 0$, the initial conditions are:

$$u_r = u_\theta = 0, \tag{98}$$

$$p(x, y, 0) = \exp\left[-\ln 2\left(\frac{(x-4)^2 + y^2}{0.04}\right)\right]. \tag{99}$$

The test problem asks for the unsteady pressure time history at three points $A(r = 5, \theta = 90°)$, $B(r = 5, \theta = 135°)$ and $C(r = 5, \theta = 180°)$, over the interval $t = 5 \rightarrow 10$.

The numerical computations were performed over the domain: $R \in [0.5, 10.5]$ and $\theta[0, 2\pi]$. For this problem three kinds of the boundary conditions are needed:

- Wall condition on the wall of the cylinder at $R = 0.5$.
- Periodic condition along both azimuthal boundaries at $\theta = 0$ and $\theta = 2\pi$.
- Outfield boundary condition, along of the far field boundary, is the acoustic radiation of Bayliss and Turkel [36].

The wall condition is based on the wall condition of Tam and Dong [37]. This requires that:

$$\frac{\mathrm{d}v_r}{\mathrm{d}t} = -\frac{\mathrm{d}p}{\mathrm{d}r} = 0. \tag{100}$$

This condition is satisfied by imposing the pressure derivatives on the wall to be zero, and $v_r = 0$ on the wall.

For this calculation, a uniformly spaced grid of 101 radial points and 153 azimuthal points was used, with a time step of CFL = 0.5. Fig. 16 shows an instantaneous pressure at $t = 7$. In this figure, the acoustic pulse is reflected by the cylinder and reaches the outer boundary. We can see that two transients are shown: the first and larger transient travels directly from the source; the second and smaller transient is reflected

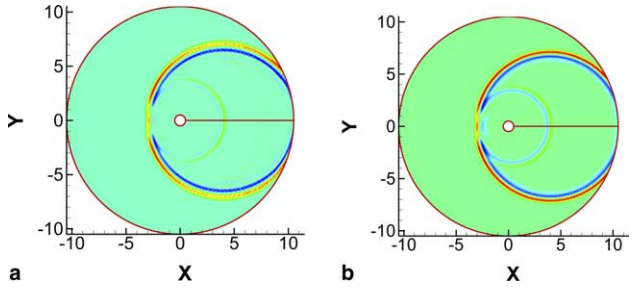

Fig. 16. Instantaneous pressure contours at time $t = 7$ – two-dimensional acoustic scattering problem. (a) DRP-fv, (b) OPC-fv.

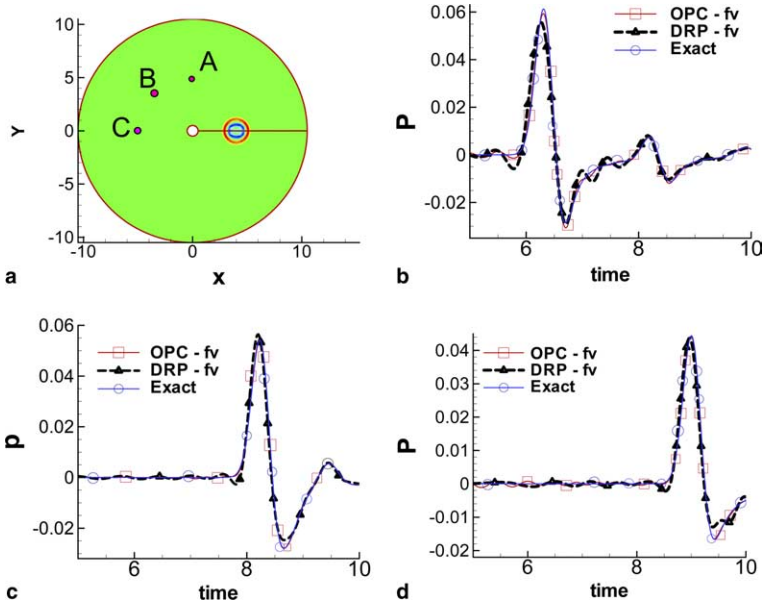

Fig. 17. The pressure history at point A, B and C – two-dimensional acoustic scattering problem: finite volume approach. (a) Position of the testing points, (b) A: $R = 5$, $\theta = 90^0$, (c) $\theta = 135°$, (d) $\theta = 90°$.

from the cylinder. Both schemes reproduce both transients with acceptable accuracy. Fig. 17 compares the solution given by the fourth-order schemes: DRP-fv and OPC-fv. Between the two schemes the OPC-fv scheme performs better.

5. Summary and conclusions

The DRP and OPC schemes, originally proposed in the finite difference form, have been assessed. To better handle nonlinearity and geometric complexities, the finite volume version of both schemes has also been developed. Linear and nonlinear wave equations, with and without viscous dissipation, have been adopted as the test problems.

For the linear wave equation with constant convection speed, the numerical stability bound posed by the CFL number is comparable between the DRP and OPC schemes. Both OPC and DRP produce solutions of a comparable order of accuracy, but the magnitude of the error of the OPC scheme is lower.

For the nonlinear wave equation, the finite volume schemes can produce noticeably better solutions and can handle the discontinuity or large gradients more satisfactorily. However, as expected, all schemes have difficulties when there is insufficient mesh resolution, as reflected in some of the short wave cases.

In conclusion, the finite volume version of both DRP and OPC schemes improves the capabilities of the original version of the finite difference formulas in regard to nonlinearity and high gradients. They can enhance performance of the original DRP and OPC schemes for many wave propagation problems encountered in engineering applications.

Acknowledgments

The NASA Constellation University Institute Program (CUIP) has partially sponsored the present work. We have benefited from communication with Profs. Chris Tam and Xin Zhang.

References

[1] J. Hardin, M.Y. Hussaini, Computational Aeroacoustics, Springer, New York/Berlin, 1992.
[2] C.K.W. Tam, J.C. Webb, Dispersion-relation-preserving finite difference schemes for computational acoustic, J. Comput. Phys. 107 (1993) 262.
[3] C.K.W. Tam, J.C. Webb, Z. Dong, A study of the short wave components in computational acoustics, J. Comput. Acoust. 1 (1993) 1–30.
[4] R. Hixon, Evaluation of high-accuracy MacCormack-type scheme using benchmark problems, NASA Contractor Report 202324, ICOMP-97-03, 1997.
[5] C. Kim, P.L. Roe, J.P. Thomas, Accurate schemes for advection and aeroacoustic, Technical Paper 97-2091, AIAA Press, Washington, DC, 1997.
[6] S.Y. Lin, Y.S. Chin, Comparison of higher resolution Euler schemes for aeroacoustics computation, AIAA J. 33 (1995) 237.
[7] W. Shyy, Computational Modeling for Fluid Flow and Interfacial Transport, Elsevier, Amsterdam, The Netherlands, 1994, revised printing 1997.
[8] W. Shyy, A study of finite difference approximations to steady-state, convection-dominated flow problems, J. Comput. Phys. 57 (1985) 415–438.
[9] F.Q. Hu, M.Y. Hussaini, J.L. Manthey, Low dissipation and dispersion Runge–Kutta for computational acoustics, J. Comput. Phys. 124 (1996) 177–191.
[10] D. Stanescu, W.G. Habashi, 2N-storage low dissipation and dispersion Runge–Kutta for computational acoustics, J. Comput. Phys. 143 (1998) 674–681.
[11] D.V. Nance, K. Viswanathan, L.N. Sankar, Low-dispersion finite volume scheme for aeroacoustic application, AIAA J. 35 (2) (1997) 255–262.
[12] G. Wang, L.N. Sankar, Prediction of rotorcraft noise with a low-dispersion finite volume scheme, AIAA-99-0480, 1999.
[13] C. Cheong, S. Lee, Grid-optimized dispersion-relation-preserving schemes on general geometries for computational aeroacoustics, J. Comput. Phys. 174 (2001) 248–276.
[14] Z.J. Wang, R.F. Chen, Optimized weighted essentially nonoscillatory schemes for linear waves with discontinuity, J. Comput. Phys. 174 (2001) 381–404.
[15] G. Ashcroft, X. Zhang, Optimized prefactored compact scheme, J. Comput. Phys. 190 (2003) 459–477.
[16] L. Tang, J. Baeder, Uniformly accurate finite difference schemes for p-refinement, SIAM J. Sci. Comput. 20 (3) (1999) 1115–1131.
[17] R. Hixon, E. Turkel, High-accuracy compact MacCormack-type schemes for computational aeroacoustic, NASA CR 1998 – 208672, 1998.
[18] H.S. Udaykumar, H.C. Kan, W. Shyy, R. Tran-Son-Tay, Multiphase dynamics in arbitrary geometries on fixed Cartesian grids, J. Comput. Phys. 137 (1997) 366–405.
[19] G. Yang, D.M. Ingram, Cartesian cut-cell method for axisymmetric separating body flows, AIAA J. 37 (1999) 905–911.
[20] H.S. Udaykumar, R. Mittal, W. Shyy, Computational of solid–liquid phase fronts in the sharp interface limit on fixed grids, J. Comput. Phys. 153 (1999) 535–574.

[21] T. Ye, R. Mittal, H.S. Udaykumar, W. Shyy, An accurate Cartesian grid method for viscous incompressible flows with complex immersed boundaries, J. Comput. Phys. 156 (1999) 209–240.
[22] D. Calhoun, R.J. Le Veque, A Cartesian grid finite-volume method for the advection–diffusion equation in irregular geometries, J. Comput. Phys. 157 (2000) 143–180.
[23] M. Popescu, W. Shyy, Assessment of dispersion-relation-preserving and space–time CE/SE schemes for wave equations, Numer. Heat Transfer 42 (2) (2002) 93–118.
[24] R.W.C.P Verstappen, A.E.P. Veldman, Numerical computation of a viscous flow around a circular cylinder on a Cartesian grid, in: European Congress Methods in Applied Sciences and Engineering, Barcelona, 11–14 September, 2000.
[25] W. Shyy, M. Francois, H.S. Udaykumar, Cartesian and curvilinear grid method for multi-domain, moving boundary domain, in: M. Debit et al. (Eds.), Thirteenth International Conference on Domain Decomposition Methods, CIMNE, Barcelona, 2001.
[26] S.C. Chang, The method of space–time conservation element and solution element methods – a new approach for solving the Navier–Stokes and Euler equation, J. Comput. Phys. 119 (1995) 295–324.
[27] S.C. Chang, X.Y. Wang, C.Y. Chow, The space–time conservation element and solution element methods: a new high-resolution and genuinely multidimensional paradigm for solving conservation laws, J. Comput. Phys. 156 (1999) 89–136.
[28] T. Ye, W. Shyy, J.N. Chung, A fixed-grid, sharp-interface method for bubble dynamics and phase change, J. Comput. Phys. 174 (2001) 781–815.
[29] C. Tannehill, D.A. Anderson, R.H. Pletcher, Computational Fluid Mechanics and Heat Transfer, Taylor & Francis, London, 1997.
[30] G. Efraimsson, G. Kreiss, A note on the effect of artificial viscosity on solution of conservation laws, Appl. Numer. Math. 21 (1996) 155–173.
[31] G. Margot, P. Olsson, Designing an efficient solution strategy for fluid flows – 1. A stable high order finite difference scheme and sharp shock resolution for the Euler equations, J. Comput. Phys. 129 (1996) 245–262.
[32] G. Efraimsson, A 2D analysis of the influence of artificial viscosity terms on solutions of the Euler equation, J. Comput. Phys. 138 (1997) 103–120.
[33] M. Sun, K. Takayama, Conservative smoothing on an adaptive quadrilateral grid, J. Comput. Phys. 150 (1999) 143–180.
[34] I. Hataue, On analogy and dissimilarity of dependence of stability on several parameters in flow simulation, J. Comput. Appl. Math. 159 (2003) 45–53.
[35] C.K.W. Tam, J.C. Hardin (Eds.), Second Computational Aeroacoustics Workshop on Benchmark Problems, NASA CP-3352, 1997.
[36] A. Bayliss, E. Turkel, J. Manthey, Far field boundary conditions for compressible flows, J. Comput. Phys. 48 (1982) 182.
[37] C.K.W. Tam, Z. Dong, Wall boundary condition for high-order finite difference schemes in computational aeroacoustics, Theor. Comput. Fluid Dyn. 6 (1994) 303.
[38] C. Bogey, C. Bailly, A family of low dispersive and low dissipative explicit schemes for flow and noise computations, J. Comput. Phys. 194 (2004) 194–214.